# Phonon replicas of charged and neutral exciton complexes in single quantum dots

D. Dufåker,[1] K. F. Karlsson,[1] V. Dimastrodonato,[2] L. O. Mereni,[2] B. E. Sernelius,[1] P. O. Holtz,[1] and E. Pelucchi[2]

[1]*Department of Physics, Chemistry, and Biology (IFM), Semiconductor Materials, Linköping University, SE-58183 Linköping, Sweden*

[2]*Epitaxy and Physics of Nanostructures, Tyndall National Institute, University College Cork, Dyke Parade, Cork, Ireland*

The longitudinal-optical (LO)-phonon coupling is experimentally examined by the optical decay of various charged and neutral exciton species in single quantum dots, and the related Huang-Rhys parameters are extracted. A positive trion exhibits significantly weaker LO-phonon replicas in the photoluminescence spectrum than the neutral and negatively charged species. Model computations show that the strength of the replicas is determined by the Coulomb interactions between electrons and holes, which modify the localization of the envelope wave functions and the net charge distribution.

## I. INTRODUCTION

Semiconductor quantum dots (QDs) are often referred to as artificial atoms since the confined charge carriers exhibit discrete energy levels similar to electrons in atoms.[1] During the last decade, remarkable technological achievements in the fabrication of QDs makes it possible to position single QDs with tailored properties in a bulk matrix with nanometric precision in all spatial dimensions.[2] This is intriguing since it allows manipulation of single atomiclike quantum states encapsulated in a well controlled solid-state environment. Therefore, QDs are good candidates as the building blocks for the next generation of electronics and photonics, relying on the laws of quantum mechanics.[3] However, unlike real isolated atoms, the QDs inevitably interact with the surrounding crystal, and the decoherence stemming from the interactions between the carriers and quantized lattice vibrations is a major issue. Dephasing due to acoustic phonons occurs rapidly on a picosecond (ps) time scale. For a polar medium, such as an InAs/GaAs QD, the optical phonons contribute to dephasing during the polaron formation process on a longer time scale ($\sim$100 ps). However, anharmonic coupling between optical and acoustic phonons accelerates the dephasing back down to a few ps.[4] It has been concluded that confinement on the nanoscale will result in an enhancement of the effective Fröhlich coupling constant;[5] a single QD provides a nearly ideal system to investigate few-particle interactions for fundamental understanding of the Fröhlich coupling.

Optically excited charge carriers may form different kinds of exciton complexes, depending on the number of electrons ($e$) and holes ($h$) trapped in the QD. However, the Fröhlich coupling between confined carriers and longitudinal-optical (LO) phonons has so far mainly been studied for the neutral exciton, formed by a single electron-hole pair. The Fröhlich coupling of the exciton is given by the difference between the couplings of the oppositely charged electron and hole.[6] For identical electron and hole probability density functions, the LO-phonon coupling vanishes due to the local charge neutrality of the QD exciton.[7] However, despite the fact that the exciton is a neutral entity, there is always a finite charge distribution in real systems due to different effective masses and confining potentials for electrons and holes. Moreover, the piezoelectric field in strained QDs separates electrons and holes and further enhances the polar coupling.[8]

In the weak-coupling regime, the LO-phonon coupling is manifested in the low-temperature optical recombination (absorption) spectrum by replicas at discrete LO-phonon energies $\hbar\omega_{LO}$ below (above) the dominating zero-phonon transition. For the independent-boson model,[9] where the electronic wave functions are assumed to remain unchanged under phonon interaction, the intensities of the LO-phonon replicas follow the Poisson distribution characterized by the Huang-Rhys parameter, describing the polar coupling strength. The experimental investigations of LO-phonon assisted recombination in III-V QDs have so far been restricted to photoluminescence (PL) spectroscopy of Stranski-Krastanow (SK) grown InAs/GaAs dot ensembles.[8] In such measurements are different exciton complexes not resolved but the average value of the Huang-Rhys parameter was extracted to be $\sim$0.015.[8] LO-phonon replicas have been resolved for single InAs/GaAs QDs in PL-excitation spectroscopy, but the coupling strength was not extracted, nor its association with charged excitonic states investigated.[10] For single CdSe/ZnCdSe QDs, data of first- and second-order LO-phonon replicas for both the exciton and the biexciton have been reported.[11] The polar coupling in such II-VI compounds is larger compared to III-V materials, and the Huang-Rhys parameter was determined to be 0.035 and 0.032 for the exciton and biexciton, respectively.[11] Thus, the investigations on the LO-phonon coupling of single QDs have so far been scanty and mainly limited to the neutral exciton (and biexciton).[6,8,11,12] Although a weak LO-phonon replica was interpreted as the signature of a neutral exciton,[10] no experimental studies compare neutral and charged exciton complexes in this regard. It was predicted theoretically, however, that an extra charge enhances the Huang-Rhys parameter by one order of magnitude for GaAs microcrystallites.[9]

In this paper, an experimental and theoretical study of the LO-phonon coupling for single pyramidal InGaAs/AlGaAs QDs is pursued. The studied pyramidal QDs are inherently site controlled and they are expected to exhibit higher symmetry ($C_{3v}$) than conventional SK QDs ($C_{2v}$), making them ideally suited as emitters of polarization entangled photon pairs.[13] Signatures of high symmetry have been reported previously for similar pyramidal QDs, demonstrating polarization isotropy of the emission,[14] very small exciton fine struc-
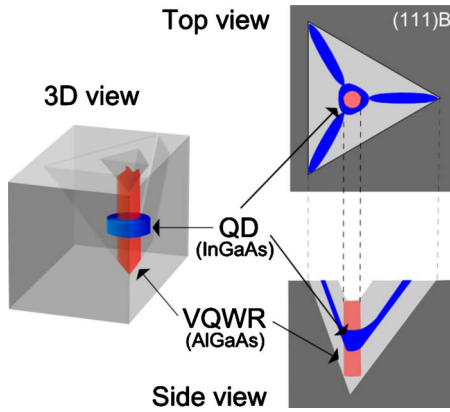
FIG. 1. (Color online) Schematic illustrations (not to scale) of the nanometric InGaAs QD (blue) and the intersecting AlGaAs VQWR (red) formed in an inverted tetrahedral micropyramid. (Right) Illustrations comprising a top view, looking down at the tetrahedral recess, and a cross-sectional side view. (Left) Oblique three-dimensional view of a cut pyramid with a cylindrical model of the QD. For a detailed geometrical description of the inverted pyramid QD system see Ref. [18].

ture splitting and emission of polarization entangled photon pairs.[15] The Huang-Rhys parameter for neutral ($X = 1e + 1h$ and $2X = 2e + 2h$), negatively charged ($X^{2-} = 3e + 1h$ and $X^{-} = 2e + 1h$), and positively charged ($X^{+} = 1e + 2h$) exciton complexes is investigated. It is demonstrated that although an extra charge strongly *enhances* the polar coupling matrix element it may lead to a significant *reduction* in the Huang-Rhys parameter.

## II. EXPERIMENTAL DETAILS

The samples were grown by metal-organic vapor phase epitaxy (MOVPE) at low pressure (20 mbar) in a commercial horizontal reactor. Standard precursors (trimethyl-aluminum/ gallium/indium and purified $AsH_3$) were used in purified $N_2$ carrier gas. The QDs were formed from a nominally 0.8-nm-thick $In_{0.15}Ga_{0.85}$ As layer in inverted tetrahedral micropyramids, patterned on a GaAs (111)B substrate with a 7.5 $\mu$m pitch. Before and after the deposition of the QD layer, the $Al_{0.30}Ga_{0.70}As$ barrier material was grown. The QDs are self-formed at the inverted tip of the tetrahedral recesses due to decomposition rate anisotropies (which lead to growth rate anisotropies) and capillarity effects.[16,17] Alloy segregation in the barrier lowers the Al concentration in the vicinity of the QD. In particular, a vertical quantum wire (VQWR) with low Al concentration ($\sim$4%) and a diameter of 16 nm is self-formed in the center of the pyramid (see Fig. 1).[19] The sample was back-etched after growth in order to enhance the light extraction efficiency.[18,20,21] Particular care on reactor handling and sources purification is necessary to obtain good quality QDs. Constant checks of the reactor status/quality were performed by routine growth of thick GaAs QWs in AlGaAs barriers as described in Refs. 22 and 23.

In a microphotoluminescence ($\mu$PL) setup the QDs were kept at a temperature of 4 or 30 K, respectively, and they were excited individually using a Ti-sapphire laser at the
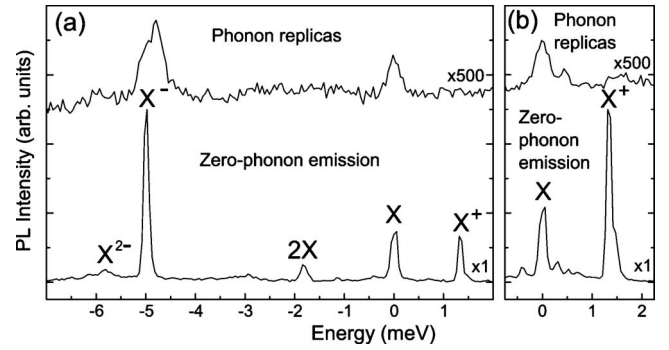


FIG. 2. $\mu$PL spectra of the direct emission and the corresponding LO-phonon replicas for QD1. The energy of $X$ is set to zero and the replicas are shifted with the phonon energy (36.4 meV). Different charging conditions are shown in (a) and (b) with dominating $X^{-}$ and $X^{+}$, respectively.

wavelength 732 nm with a spot size of $\sim$1.5 $\mu$m. A single grating monochromator (1200 grooves/mm, focal length 0.55 m) equipped with a charge coupled device (CCD) camera was used to acquire the single QD spectra with a spectral resolution of 0.1 meV. In order to achieve the dynamical range required to simultaneously detect signals which differ by three orders of magnitude, half of the CCD chip was dimmed by a neutral density filter transmitting 1.46%. The dimmed part recorded the zero-phonon recombination while the unshaded part recorded the much weaker phonon replicas.

## III. RESULTS AND DISCUSSION

The average number of electrons and holes populating the QDs is controlled by the excitation conditions such as excitation power and crystal temperature. Various exciton complexes were spectrally identified in accordance with earlier works on similar QDs.[24–26] $\mu$PL spectra for one QD (QD1) are shown in Fig. 2, where $X^{-}$ dominates the zero-phonon PL spectrum at low excitation power, $\sim$20 nW [Fig. 2(a)] and $X^{+}$ dominates at higher power, $\sim$60 nW [Fig. 2(b)]. The energy scale of Fig. 2 is chosen such that the emission of $X$ at 1440 meV is set to zero. The weak multipeak structure near $X$ and the high-energy small shoulder of $X^{+}$ in Fig. 2(b) occurs only when the dot is strongly positively charged. These features are tentatively attributed to multicharged excitons (e.g., $X^{2+} = 1e + 3h$). The first-order phonon assisted recombination occurs at a phonon energy $\hbar\omega_{LO}$ below the zero-phonon emission. The corresponding spectra are also displayed in Fig. 2, shifted in energy by $\hbar\omega_{LO} = 36.4 \pm 0.1$ meV, for convenient comparison. Note that the phonon replica spectra always are dominated by $X$ or $X^{-}$, also for the case of a strongly positively charged QD [Fig. 2(b)]. The signal-to-noise ratio did not allow detection of the second order phonon replicas but it was concluded that these second-order replicas are at least 20 times weaker than the first-order replicas.

The Huang-Rhys parameter for the charged and neutral excitons of QD1 has been extracted from several sets of $\mu$PL spectra, e.g., as presented in Fig. 2, and the obtained aver-
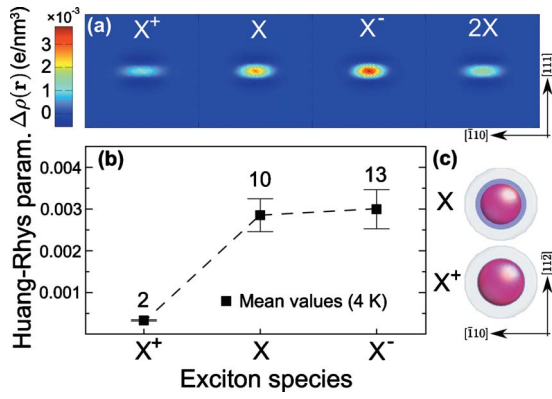
FIG. 3. (Color online) (a) Computed differences in the charge distributions of the excitonic initial and final states shown in a vertical plane across the QD center (piezoelectric field excluded). (b) Measured Huang-Rhys parameters for QD1, represented by mean values of several measurements. The bars indicate one standard deviation from the mean, and the numbers above indicate the number of measurements. The dashed line serves as a guide to the eyes. (c) Computed isosurfaces of electron (hole) envelope probability density functions [10% of maximum] for $X$ and $X^+$ shown in blue (red). The InGaAs QD geometry is shown in gray.

aged values are plotted in Fig. 3(b). It is clear that the Huang-Rhys parameter of $X^+$ is significantly lower than for $X$ and $X^-$. This trend is common for all QDs measured [see Fig. 4(b) for a summary of data for 17 measured QDs]. It should be noted that there are significant dot-to-dot variations in the Huang-Rhys parameter, as represented by the error bars of Fig. 4(b). For one QD the temperature was raised to 30 K in order to make the biexciton $2X$ dominate the zero-phonon emission. The so extracted value of the Huang-Rhys parameter is also significantly smaller than for $X$ and $X^-$. Furthermore, the spectral linewidths of the phonon replicas are considerably larger than the corresponding zero-phonon emission (see Fig. 5).

In contrast to $X$, the phonon replicas of a complex formed by more than one electron and one hole are not given strengths only by the charge distribution of the initial state but also by the final state. Thus, except for $X$, the Huang-Rhys parameter, which is extracted from the optical excitonic transitions, is consequently not a measure of the polar coupling of the initial excitonic state. The fact that the replica of $X^+$ is particularly weak can be qualitatively understood as the hole is heavier and, thus, more localized than the electron. When an additional hole is added to the neutral electron-hole pair ($X$), the Coulomb repulsion between the two holes will expand their respective distribution in space while the additional attraction caused by the extra hole on the electron will reduce the extent of the negative charge distribution. In this way the holes become more delocalized while the electron becomes more localized in the case of $X^+$, in comparison to $X$. Thus, the Coulomb interaction reduces the difference in electron and hole distributions for $X^+$, making the net charge of an electron-hole pair nearly vanishing. Consequently, the space charge of $X^+$ is very close to the space charge of a single hole, i.e., the final state of the optical transition. Similar arguments were elaborated in Ref. 27 to explain why $X^+$
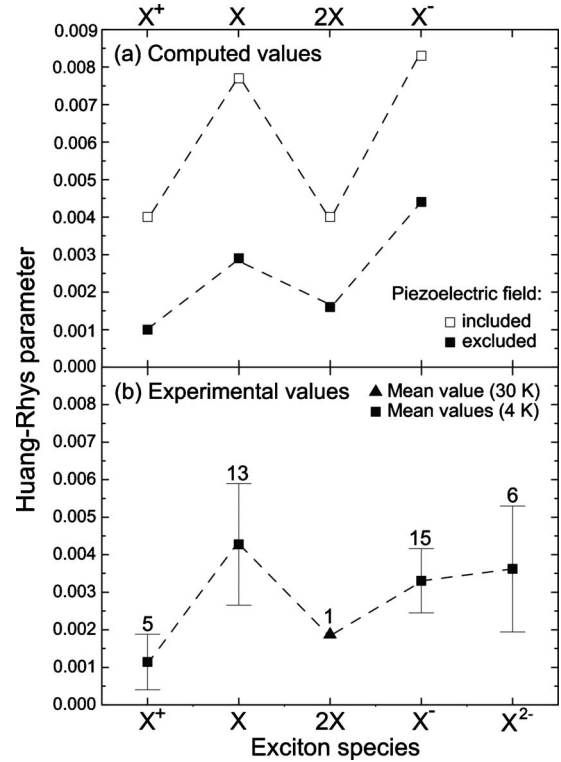


FIG. 4. (a) Computed and (b) measured values of the Huang-Rhys parameter. The experimental data are averaged for different QDs with bars indicating one standard deviation from the mean and the number above indicate the number of measured QDs. Note that $2X$ was measured for only one QD but the value is averaged from several spectra. The theoretical values were obtained by either including or excluding the piezoelectric field. The dashed lines serve as guides to the eyes.

exhibits smaller permanent exciton dipole than $X$.

In order to quantitatively determine the charge distributions of the initial and the final states for the excitonic transitions, the $8 \times 8$ band $\mathbf{k} \cdot \mathbf{p}$ theory[28,29] was used for self-consistent numerical computations of the electron and hole wave functions in the Hartree approximation, where many-particle correlations and exchange interactions are neglected.
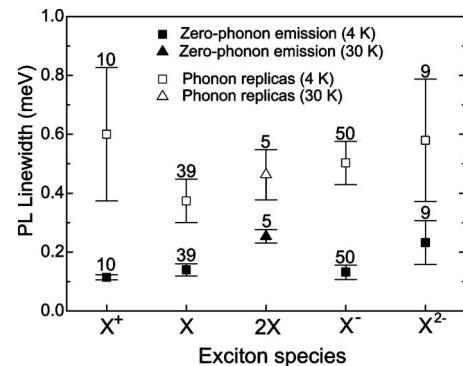


FIG. 5. The measured linewidth (full width at half maximum) represented by the mean values of in total 17 different QDs. The bars indicate one standard deviation from the mean, and the numbers above indicate the number of measurements.

The QD is modeled as an InGaAs disk of thickness (diameter) 6 nm (24 nm) in which the In concentration is assumed to decrease from 20% in the center to 10% at the perimeter, in order to account for In segregation [see Fig. 1 (left)]. The Al concentration in the AlGaAs barriers is chosen to be 25%, and a VQWR with 5% Al and 16 nm diameter intersects the QD. The model takes into account the deformation of the potential due to strain by the continuum elastic theory. The computed transition energy for $X$ at 1436 meV is close to the corresponding measured PL energies for the investigated QDs.

The computed differences in the charge distribution $\Delta\rho(\mathbf{r})$ between the initial and the final states for some relevant excitonic transitions are shown in Fig. 3(a). The corresponding electron and hole distributions of the initial states for $X$ and $X^+$ are shown in Fig. 3(c). As expected from the above-mentioned qualitative arguments, the smallest magnitude of $\Delta\rho(\mathbf{r})$ is obtained for $X^+$. Similar qualitative arguments can be made for $X^-$ to explain why $\Delta\rho(\mathbf{r})$ should increase for $X^-$ compared to $X$. For $2X$, two additional and oppositely charged carriers are added to the neutral exciton $X$ and the competing effects of delocalization (from adding a charge carrier with equal charge) and localization of the envelope wave functions (from adding a charge carrier of opposite charge) eventually result in a magnitude of $\Delta\rho(\mathbf{r})$ significantly lower than for both $X$ and $X^-$.

The independent-boson model is used to compute the Huang-Rhys parameter from the Fourier transform of $\Delta\rho(\mathbf{r})$.[9] This adiabatic approach neglects phonon-induced scattering between the electronic states. Such a crude approximation is not always valid for QDs.[12] In particular, the second-order phonon replicas and the excited states may be altered by nonadiabatic effects.[6] Therefore, our analysis is limited to the first-order phonon replicas of complexes with all carriers in the single-particle ground states.

The computed Huang-Rhys parameters for the relevant exciton species are shown in Fig. 4(a). Two sets of values are obtained by either excluding or including the strain-induced piezoelectric field, as computed by numerically solving the Poisson's equation with the charge density obtained from the piezoelectric polarization using the first-order piezoelectric tensor.[30,31] The vertical electric field ($\sim100$ kV/cm) separates the electrons and the holes and results in a less efficient cancellation of the positive and negative charges leading to stronger phonon replicas. However, it should be noted that the value of the piezoelectric constant for the InGaAs QD is controversial, and the effects of second-order terms may be important.[32] Moreover, the reason for the factor of 2 larger magnitude of the electric fields computed by continuum models compared to what is obtained with atomistic approaches,[33] using the same piezoelectric constants, still remains to be explained. There are therefore good reasons to believe that the piezoelectric field in the real QDs is lower than the value computed here.

The theoretically computed values of the Huang-Rhys parameter are in fair agreement with the experimental data (see Fig. 4). For $X^+$, $X$, and $2X$ the experimental values falls between the computed values with and without the piezoelectric field. However, the larger Huang-Rhys parameter predicted for $X^-$ compared to $X$ cannot be experimentally verified due to the uncertainties in the measured values. The large dot-to-dot variation is tentatively attributed to sensitiveness of the Huang-Rhys parameter on the electric fields, which may vary slightly with the local environment for each QD. Note that the Huang-Rhys parameter of $X$ obtained here for the pyramidal $In_{0.15}Ga_{0.85}As/AlGaAs$ QDs is only 20–30 % of the values reported for InAs/GaAs SK QDs on (001) substrates.[8] Lower values are not surprising since a lower In-concentration results in a weaker piezoelectric field. Moreover, for the high-symmetry pyramidal QDs, the piezoelectric field is directed vertically along the smallest dimension of the QD while for the low-symmetry SK QDs, grown on the (001) plane, the field is also acting laterally. Thus, the strong lateral deformation of the electron and hole wave functions present in the SK QDs,[8] dramatically enhancing the Huang-Rhys factor for dots with a wide base, is not present in the pyramidal QDs.

According to the discussion above, the integrated squared modulus of the diagonal polar coupling matrix element alone determines the strength of the phonon replicas solely for $X$. It is therefore interesting to compare the computed integral for $X$ with the corresponding ones for $X^+$, $2X$, and $X^-$. The obtained values are 23, 3, and 14 (10, 3, and 6) times larger than for $X$, respectively, excluding (including) the piezoelectric field. Thus, $X^+$ exhibits *strongest polar coupling* and simultaneously displays the *weakest LO-phonon replica* upon decay.

The measured average energy of the LO phonon is $\hbar\omega_{LO}=36.4\pm0.1$ meV which is slightly lower than 36.6 meV corresponding to bulk LO-phonon energies in GaAs.[34] Surface optical phonon modes at the interface between the dot and the surrounding lattice can be neglected due to the small dielectric contrast between the QD and the barrier in the studied structure.[35] Instead, the measured value of $\hbar\omega_{LO}$ energy is reasonably related to the InGaAs QD or the AlGaAs barriers. Increasing the Al concentration from 0% to 4% downshifts the GaAs-like bulk mode in AlGaAs by 0.2 meV.[30] Thus, the estimated LO-phonon frequency of the VQWR is 36.4 meV, if phonon confinement is neglected while other parts of the AlGaAs barrier (Al concentration 20–30 %) exhibit $\hbar\omega_{LO}$ in the range 35.0–35.5 meV. Similarly, the expected GaAs-like LO-phonon energy of unstrained $In_{0.15}Ga_{0.85}As$ is 35.9 meV.[36] The compressive strain present in the QD splits the degenerate phonon modes and shifts the energies up by 0.4–0.8 meV, as estimated from the computed strain tensor using the theory and parameters of Refs. 37 and 38. Thus, the decay of exciton complexes excites LO phonons either in the InGaAs QD or in the AlGaAs VQWR, and the estimated phonon energies are near 36.4 meV for both structures.

Finally, the spectral linewidth of the phonon replicas will be addressed. By including bulklike phonon dispersion in the model,[39] the replicas broaden by less than 50 $\mu$eV. Furthermore, the intrinsic LO-phonon lifetime in GaAs yields a linewidth of $\sim70$ $\mu$eV.[40] This does not explain the measured linewidths of 400–600 $\mu$eV for the LO-phonon replicas (Fig. 5). Additional broadening is however expected from the composition variations and alloy disorder.[41] From the analysis of the LO phonon energies above, it is clear that a variation in the In or Al concentration by $\sim2$% corresponds to a

phonon energy variation of $\sim$0.1 meV. Although the exact variation in the In (Al) composition in the QD (VQWR barrier) is not known, variations by several percent are expected. Moreover, the inhomogeneous strain field in the QD splits the phonon modes by $\sim$0.4 meV and gives rise to additional broadening by $\sim$0.1 meV.[37,38] It is worth to mention that some replicas exhibit resolved shoulders or double peaks [e.g., for of $X^-$ in QD1 shown in Fig. 2(a)], which can be interpreted as a strain-induced splitting of the phonon modes.

## IV. CONCLUDING REMARKS

The LO-phonon assisted recombination has been investigated for individual pyramidal InGaAs QDs and for specific exciton species ($X^+$, $X$, $2X$, $X^-$, and $X^{2-}$). It was demonstrated that extra charge trapped in the QD does not result in any dramatic enhancement of the LO-phonon replicas. In contrast, $X^+$ which exhibits the strongest polar coupling among the theoretically studied complexes, displays the weakest LO-phonon replica in both experiments and computations. The values of the Huang-Rhys parameters obtained with the independent-boson model are in fair agreement with experiments. The computations show that the Coulomb-induced

charge cancellation of the electron-hole pair, in the presence of an extra hole, is responsible for the reduced intensity of the LO-phonon replica of $X^+$. A similar charge cancellation was found to reduce the permanent exciton dipole for positively charged excitons in conventional SK QDs.[27] It is therefore expected that our reported charge dependence of the Huang-Rhys parameter also is valid for SK QDs. We hope that our results will inspire further measurements of the phonon replicas for other classes of QDs, and also stimulate the implementation of nonadiabatic many-body models for a more sophisticated theoretical description of the phonon interaction with exciton complexes.

[1] D. Gammon, Nature (London) **405**, 899 (2000).

[2] P. Gallo, M. Felici, B. Dwir, K. A. Atlasov, K. F. Karlsson, A. Rudra, A. Mohan, G. Biasiol, L. Sorba, and E. Kapon, Appl. Phys. Lett. **92**, 263101 (2008).

[3] X. Li, D. Steel, D. Gammon, and L. J. Sham, Opt. Photonics News **15**, 38 (2004).

[4] L. Jacak, J. Krasnyj, W. Jacak, R. Gonczarek, and P. Machnikowski, Phys. Rev. B **72**, 245309 (2005).

[5] L. Jacak, J. Krasnyj, and W. Jacak, Phys. Lett. A **304**, 168 (2002).

[6] O. Verzelen, R. Ferreira, and G. Bastard, Phys. Rev. Lett. **88**, 146803 (2002).

[7] S. Schmitt-Rink, D. A. B. Miller, and D. S. Chemla, Phys. Rev. B **35**, 8113 (1987).

[8] R. Heitz, I. Mukhametzhanov, O. Stier, A. Madhukar, and D. Bimberg, Phys. Rev. Lett. **83**, 4654 (1999).

[9] S. Nomura and T. Kobayashi, Phys. Rev. B **45**, 1305 (1992).

[10] P. Hawrylak, G. A. Narvaez, M. Bayer, and A. Forchel, Phys. Rev. Lett. **85**, 389 (2000).

[11] F. Gindele, K. Hild, W. Langbein, and U. Woggon, Phys. Rev. B **60**, R2157 (1999).

[12] V. M. Fomin, V. N. Gladilin, J. T. Devreese, E. P. Pokatilov, S. N. Balaban, and S. N. Klimin, Phys. Rev. B **57**, 2415 (1998).

[13] K. F. Karlsson, M. A. Dupertuis, D. Y. Oberli, E. Pelucchi, A. Rudra, P. O. Holtz, and E. Kapon, Phys. Rev. B **81**, 161307(R) (2010).

[14] K. F. Karlsson, V. Troncale, D. Y. Oberli, A. Malko, E. Pelucchi, A. Rudra, and E. Kapon, Appl. Phys. Lett. **89**, 251113 (2006).

[15] A. Mohan, M. Felici, P. Gallo, B. Dwir, A. Rudra, J. Faist, and E. Kapon, Nat. Photonics **4**, 302 (2010).

[16] G. Biasiol, A. Gustafsson, K. Leifer, and E. Kapon, Phys. Rev. B **65**, 205306 (2002).

[17] E. Pelucchi, S. Watanabe, K. Leifer, Q. Zhu, B. Dwir, P. D. L. Rios, and E. Kapon, Nano Lett. **7**, 1282 (2007).

[18] A. Hartmann, Y. Ducommun, K. Leifer, and E. Kapon, J. Phys.: Condens. Matter **11**, 5901 (1999).

[19] Q. Zhu, E. Pelucchi, S. Dalessi, K. Leifer, M.-A. Dupertuis, and E. Kapon, Nano Lett. **6**, 1036 (2006).

[20] L. O. Mereni, V. Dimastrodonato, R. J. Young, and E. Pelucchi, Appl. Phys. Lett. **94**, 223121 (2009).

[21] V. Dimastrodonato, L. O. Mereni, R. J. Young, and E. Pelucchi, Phys. Status Solidi B **247**, 1862 (2010).

[22] E. Pelucchi, N. Moret, B. Dwir, D. Y. Oberli, A. Rudra, N. Gogneau, A. Kumar, E. Kapon, E. Levy, and A. Palevski, J. Appl. Phys. **99**, 093515 (2006).

[23] V. Dimastrodonato, L. Mereni, R. J. Young, and E. Pelucchi, J. Cryst. Growth **312**, 3057 (2010).

[24] A. Hartmann, Y. Ducommun, E. Kapon, U. Hohenester, and E. Molinari, Phys. Rev. Lett. **84**, 5648 (2000).

[25] V. Troncale, K. F. Karlsson, D. Y. Oberli, M. Byszewski, A. Malko, E. Pelucchi, A. Rudra, and E. Kapon, J. Appl. Phys. **101**, 081703 (2007).

[26] M. H. Baier, A. Malko, E. Pelucchi, D. Y. Oberli, and E. Kapon, Phys. Rev. B **73**, 205321 (2006).

[27] J. J. Finley *et al.*, Phys. Rev. B **70**, 201308(R) (2004).

[28] E. O. Kane, *Band Theory and Transport Properties, Handbook on Semiconductors* (North-Holland, Amsterdam, 1982), Vol. 1.

[29] I. Vurgaftman, J. R. Meyer, and L. R. Ram-Mohan, J. Appl. Phys. **89**, 5815 (2001).

[30] S. Adachi, J. Appl. Phys. **53**, 8775 (1982).

[31] M. Grundmann, O. Stier, and D. Bimberg, Phys. Rev. B **50**, 14187 (1994).

[32] G. Bester, X. Wu, D. Vanderbilt, and A. Zunger, Phys. Rev. Lett. **96**, 187602 (2006).

[33] S. P. Łepkowski, Phys. Rev. B **77**, 155327 (2008).

[34] G. Irmer, M. Wenzel, and J. Monecke, Phys. Status Solidi B **195**, 85 (1996).

[35] D. V. Melnikov and W. B. Fowler, Phys. Rev. B **64**, 245320 (2001).

[36] J. Groenen, R. Carles, G. Landa, C. Guerret-Piécourt, C. Fontaine, and M. Gendry, Phys. Rev. B **58**, 10452 (1998).

[37] F. Cerdeira, C. J. Buchenauer, F. H. Pollak, and M. Cardona, Phys. Rev. B **5**, 580 (1972).

[38] P. Wickboldt, E. Anastassakis, R. Sauer, and M. Cardona, Phys. Rev. B **35**, 1362 (1987).

[39] D. Strauch and B. Dorner, J. Phys.: Condens. Matter **2**, 1457 (1990).

[40] M. Canonico, C. Poweleit, J. Menéndez, A. Debernardi, S. R. Johnson, and Y.-H. Zhang, Phys. Rev. Lett. **88**, 215502 (2002).

[41] B. Jusserand and J. Sapriel, Phys. Rev. B **24**, 7194 (1981).